Energetic Consequences of Series and Parallel Springs in Lower-Extremity Powered Prostheses

Matthew E. Carney,[1] *Member, IEEE,* Hugh Herr,[1]

***Abstract*—We present electric energetic consequences for mechanical design trade-offs in lower-extremity powered prostheses. There are four main hardware components commonly implemented in these devices that can be tuned to achieve desired performance: motor, reduction ratio N, series spring stiffness K_s, and parallel spring stiffness K_p. The allowed joint range of motion is a fifth parameter that can also drastically change energy consumption. We apply a kinematically clamped analysis to the system equations to map the electric cost of transport (COT) for knee and ankle level-ground walking, in addition to ankle stair ascent and descent. We also utilize an optimization procedure to identify minimum energy hardware configurations. The energy map provides insight into consequences of variance from optimal parameters. Our results support the contribution of the series elastic element for improved power output. Parallel stiffness can provide $\leq$8% improvements in walking with minimal negative effect with varied terrain, and a varying ankle transmission ratio can similarly improve COT by $\leq$8% from level-ground to stair ascent. Limited dorsiflexion can further improve COT by 30%. These observations can provide the designer clarity to how design decisions modulate hardware performance.**

***Index Terms*—robotics, prostheses, actuator, ankle, knee.**

I. Introduction

THE motivation to build powered ankle prostheses is to generate the roughly 0.2 J/kg net positive work done by the ankle during walking that cannot be provided by a traditional ankle-foot prosthesis [1], [2]. Providing this energy can reduce the energetic cost of walking [3]–[5], improve qualitative feel and ground control, reducing falls, and normalizing gait to reduce social stigma of pathological gaits as well as early onset of co-morbidities [6]. Though the knee operates primarily as an energy absorber during walking, co-morbidities and pathologies, similar to the ankle, can potentially be avoided with the dynamic control of powered devices throughout swing and stance phases.

Mimicking nature with synthetic hardware is a capability that our field is closely approaching. The mechanical design trade-offs pose challenges that differ between academic and commercial applications. The commercial-off-the-shelf powered ankle and knee systems are not able to provide biologically accurate kinetics with kinematics, nor do they enable access to the underlying control systems [7], [8]. To improve upon the commercial options, a growing handful of academic research groups around the world have been building individualized platforms for study, all with their own trade-offs.

The first powered ankle, published by Au, Weber, Herr, used a series elastic actuator (SEA) [9] configured with a parallel spring to improve torque bandwidth in the transition from controlled dorsiflexion to powered-push-off. Au *et al.* showed that their actuator's ability to contribute energy during powered push-off improved the metabolic cost of walking [10]. Since then numerous actuators have been designed following a similar actuator topology [11]–[15]. Many of these designs have focused around flat, level-ground walking, where primary kinetic behavior occurs as a large power maneuver during powered plantar flexion.

The series elastic actuator (SEA) [9] has been the core actuator technology for the design of powered prostheses due to its energetically favorable features of a contractile element in series with an elastic element. This configuration of spring is a biomimetic representation of the biological muscle and tendon unit [16]. The SEA has a number of benefits that include: reduced impact loading on drivetrain, force control from position measurement and control, decoupling of drivetrain impedance from output impedance, and the ability to deliver more power than a motor alone when operated as slingshot [17]. The parallel element has been used to improve control bandwidth and energetics in level-ground walking [3], [12], [18]. However, the parallel element also increases system complexity and mass. To determine the efficacy of the parallel spring for our application we analyzed its energetic contributions during walking and extended these effects to uneven terrain.

Reductions in metabolic Cost of Transport (COT) for people with lower-extremity limb differences wearing powered prostheses compared to those with conventional passive devices has been accomplished [3]. However, differing results of metabolic energy benefits from such devices have also been reported [5], [19]–[21]. Even in results that have shown metabolic improvements, the energy cost of walking still remains greater than that of un-affected persons, particularly at common self-selected walking speeds and faster [4], [5], [22]; the field has struggled to reduce the metabolic cost of walking with powered prostheses, tethered or not.

These limitations in clinical studies may be due to differences between machine and biological kinetic and kinematic capabilities, along with the distal mass of such devices. Many clinical energetic studies have used the commercial product BiOM from BionX which has limited range-of-motion (ROM)

Manuscript received Month, Year.

Financial support: this work was supported in part by the MIT Media Lab Consortia, the U.S. Army Medical Research and Materiel Command (W81XWH-14-C-0111) and the Defense Advanced Research Projects Agency (W911NF-17-2-0043).

[1]MIT Center for Extreme Bionics and MIT Media Lab - Biomechatronics Group, Massachusetts Institute of Technology, Cambridge, MA 02139 USA. e-mail: mcarney@mit.edu.

Fig. 1. The TF8 Actuator is designed to operate as either a knee or ankle actuator – shown here configured as an ankle prosthesis. Borrowed with permission from [24].

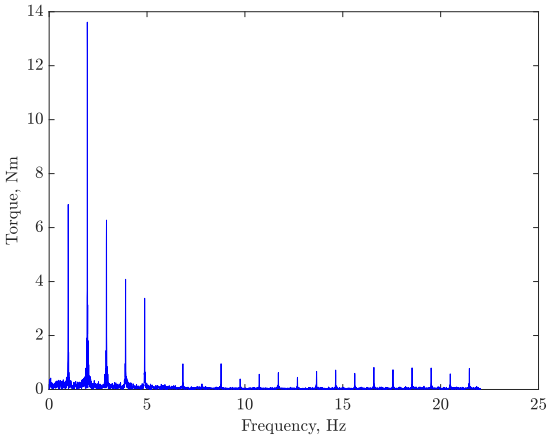

Fig. 2. Power spectral analysis of knee torque contributions up to 70 % of the joint power during a gait cycle of a 90 kg person walking at 2 m/s. Knee torque frequency contributions amount to 73 Nm at 6 Hz with a maximum torque of 118 Nm.

from zero dorsiflexion to twenty-five degrees plantar flexion and a mass of 2.3kg [7]. Though well designed for energy efficient level-ground walking, these systems quickly hit kinematic limits at higher walking velocities and varied terrain, where joint angle extension increase [23].

In this study we aim to elucidate how the common trade-offs in the mechanical design of lower-extremity powered prostheses affect overall system performance. We provide our process for evaluating the design space and searching for minimum energy combinations of motors, reduction-ratios, series and parallel stiffness, and joint range of motion limits. We then apply these tools to evaluate ankle prostheses walking on stairs in addition to level-ground, as well as knee actuators during level-ground walking. Application of these results in built hardware, Fig. 1 are presented in an accompanying mechatronic design paper [24], separated for clarity.

II. Methods

Understanding the energetic consequences of design variables leads to higher performance hardware and improved design for application specificity. For this application we initiated the design assuming series elasticity would be included as a mechanical energy storage mechanism, as has been done by many researchers of ambulating robotics. Following a process similar to [25]–[27] we evaluated the performance of a SEA kinematically clamped to mean biological gait data while searching for drivetrain component specifications for a series spring, motor, reduction ratio and in some cases unidirectional parallel springs that satisfy the search objective and system constraints. We also performed wider design space evaluation of the energetic consequences each of these hardware components to help understand the consequences of design decisions on stairs in addition to level-ground walking.

A. Design Specification

To determine the design specification for range of motion, torque, power, and system bandwidth, we normalized and scaled by body mass mean gait data from a total of one thousand unique gait cycles of walking data from nine able-bodied subjects collated from [28]. In addition to walking, mean stair ascent and descent ankle trajectories from [29] are used to evaluate energetics of stairs. We set a performance target and evaluated component contributions based on a 90 kg user walking at a near jogging pace of 2.0 m/s.

The widely accepted measure of an actuator's ability to achieve a desired performance is the torque bandwidth: a measure of the ability of an actuator to assert a specified torque at a specified velocity. Much of the literature states the ankle bandwidth design requirement is 2-4 Hz at 50-140 Nm torque for human level-ground walking. This specification originates with [10], where they defined bandwidth as a frequency range within which 70 % (3 dB range) of the system energy is contained when evaluated with Parseval's Theorem.

To evaluate torque bandwidth for more complex trajectories other than the ankle such as the knee, or other arbitrary joint trajectories we used the [10] method and expanded it to determine a generalized bandwidth magnitude requirement. The sum of peaks over 2.5 % of the maximum absolute torque spectral density were then summed and the maximum frequency of these torque contributions were taken as the frequency bandwidth. This method was verified against the [10] method applied to a 75 kg 1.25 m/s walking able-bodied subject. Shown in Fig. 2is collected from the [28] knee torque trajectories scaled to a 90 kg user walking at 2 m/s. The result is a desired frequency bandwidth of 73 Nm at 6 Hz. The specificity of this method is somewhat misleading due to its frequency domain approach to analysis of an entire gait cycle, rather than true time-domain features. Nonetheless, this method provides an effective estimation point.

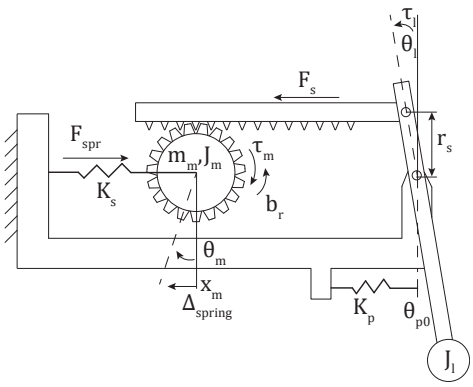

Fig. 3. Schematic of the series elastic actuator and parallel elastic element used for the design process (rack-pinion model adapted from [31]). Our coordinate frame assumes ankle angle and torque do positive work on the environment – plantarflexion is positive; for knee flexion angle and torque is also positive.

B. Modeling and Optimization

To model the mechanical and electrical systems dynamics we used a kinematically clamped analysis method where the actuator output explicitly tracks the prescribed joint load torque, angle and velocity trajectories [25], [27], [30]. Linearized kinematic and electric dynamic models clamped to these vectors output: motor, power electronics and spring behavior. These models do not include non-linear viscous friction terms but the search method does include saturation constraints on motor torque, velocity, current, and voltage. The result is a model that generally trends correctly but is operating in an open-loop dynamic condition with minimal damping, thereby potentially exhibiting large velocity response at impact conditions e.g. parallel spring engagement or ground contact. Mean torque, velocity, and angle trajectories aggregated from [28] were mass normalized, scaled, and fed into the dynamic equations for a series elastic actuator.

Kinematic analysis from free body and mass acceleration diagrams of the joint components give the following equations that reference Fig. 3:

$$\tau_l = \tau_s + \tau_p - J_l\ddot{\theta}_l \tag{1}$$

where,

$$\tau_s = r_s F_s = r_s K_s(\frac{\theta_m}{N} - r_s\theta_l) \tag{2}$$

$$\tau_p = \begin{cases} -K_p(\theta_l - \theta_{p_0}), & \theta_l < \theta_{p_0} \\ 0, & \theta_l >= \theta_{p_0} \end{cases} \tag{3}$$

and where, joint load is τ_l, the unidirectional parallel spring contribution is τ_p, the parallel spring rate is K_p, the parallel spring engagement point is θ_{p_0}, the series elastic actuator torque contribution is τ_s, the load inertia is J_l and load acceleration is $\ddot{\theta}_l$. In the case of the knee J_l assumes a point mass of an equivalent leg segment [32] located one third of a leg distance away from the knee joint. Positive joint angle and torque is in the plantarflexion direction, based on a reference that positive work is done to the environment. The load inertia is not necessarily known as it changes through stance and swing phases; for this analysis inertia was assumed operating in free-space and used equivalent leg segment mass as defined in [24] for the ankle or knee analyses depending on the mass of the next distal link. Here r is the moment arm acted on by the linear actuator force F_s at the joint axis. This moment arm r_s was initially held constant, but later as the actuator topology evolved to include a linkage geometry, the moment arm became a function $r_s(\theta_l)$. The motor position is θ_m, and the drivetrain reduction ratio is $N = N_s r_s$, where for the case of the ballscrew $N_s = \frac{2\pi}{lead}$. Plugging τ_s and τ_p into equation (1), and rearranging, the force in the series spring actuator is F_s:

$$F_s = \frac{1}{r_s}[\tau_l - K_p(\theta_l - \theta_{p_0}) + J_l\ddot{\theta}_l] \tag{4}$$

Passing this force through the transmission results in an effective torque that the motor sees:

$$\tau_m = (J_m + J_{tr})\ddot{\theta_m} + b_m\dot{\theta}_m + \frac{F_s}{N_s} \tag{5}$$

$$b_m = \frac{K_t I_{nl}}{\omega_{nl}} + b_r \tag{6}$$

where, J_m is motor rotor inertia and J_{tr} is transmission inertia. Along with the motor and transmission inertias, the damping term b_m given by [33] represents viscous friction in the motor, where K_t is motor constant, $I_n l$ is no-load current, ω_{nl} is no-load speed, and b_r is viscous damping in the drivetrain and rolling elements estimated based on [3]. Rearranging (2) to solve for motor angle θ_m gives:

$$\theta_m = N(\frac{F_s}{K_s} + r_s\theta_l) \tag{7}$$

In accounting for drivetrain inefficiencies motor torque is adjusted by an estimated transmission efficiency that biases motor torque by the bidirectional power flow [33]. Four quadrant motor control is assumed and the power electronic efficiency is included in the piecewise continuous power efficiency term, η:

$$P_{mech} = \tau_m\dot{\theta}_m \tag{8}$$

$$\tau_m = \begin{cases} \tau_m \cdot \eta, & P_{mech} < 0 \\ \tau_m \cdot \frac{1}{\eta}, & P_{mech} > 0 \end{cases} \tag{9}$$

Torque and angle at the motor are then fed into the linearized electromagnetic model of the motor to determine required current and voltage in the motor windings, shown below. The electrical power flow through the motor is integrated over a gait cycle to determine the electric energy consumed by the motor to produce the specified torque and velocity trajectory:

$$i_m = \frac{\tau_m}{K_t} \tag{10}$$

$$v_m = i_m R_m + K_t\dot{\theta}_m + \frac{di}{dt}L \tag{11}$$

$$P_m = i_m v_m \tag{12}$$

where, i_m, v_m, P_m are motor current, voltage, and power respectively. R_m is motor winding resistance, and L is winding inductance.

To identify the necessary operating parameters for powered prosthesis joint actuators, we used an optimization process

similar to [25], [26]. The search objective was to minimize the electrical COT per gait cycle, subject to physical constraints such as motor and power electronics capabilities. To identify ideal component parameters we applied a gradient descent optimization procedure with non-linear constraints imposed by the motor and power electronics:

$$COT = \frac{\int P_m(t)dt}{\frac{1}{2}mg \cdot \Delta x} \tag{13}$$

$$\begin{aligned} \min \quad & COT && (14)\\ \text{s.t.} \quad & |\tau_m| - \tau_{allow} \leq 0 && (15)\\ & |\omega_n| - \omega_{n_{des}} \leq 0 && (16) \end{aligned}$$

where, ω_n is lumped-mass natural frequency of the motor and drivetrain [9], [31]. For motors with limited manufacturer data availability the following relations are used to estimate motor capabilities:

$$\tau_{allow} = -\frac{\tau_o}{\omega_o}|\dot{\theta}_m| + \tau_o \tag{17}$$

where, τ_o and ω_o are stall torque and no-load speed, or the maximum values given by the manufacturer. Finally, we aggregated the results and sorted them by minimum electric energy consumption across all the design parameters.

C. Static Evaluation

An initial guess at potential motor candidates and parallel spring stiffness can be estimated by inspection of static parameters.

A first estimate of a parallel spring stiffness comes from a static inspection of 1 and 3. In a static condition we can neglect the inertial contribution. With the goal of reducing load on the motor, the torque contribution τ_s is negated, and we set τ_p to equal τ_l, such that:

$$K_p = \frac{min(\tau_l)}{min(\theta_l - \theta_{po})} \tag{18}$$

.

To compare motor capabilities we need to evaluate the motor torque generating efficiency in relation to the effect of rotor inertia and the expected reduction ratio. The *motor constant*:

$$K_m = \frac{K_t}{\sqrt{R}} \tag{19}$$

with units $[\frac{Nm}{\sqrt{W}}]$, can be used to compare motor torque generation efficiency, where, R is motor winding resistance, and K_t is torque constant with units $[Nm/A]$. Though, because this measure misses the effects of rotor inertia, Sensinger defined the *Speed Rate* as a benchmark to use in evaluating motor dynamic performance by normalizing the motor constant with rotor inertia [34]. However, this term does not consider the effect of drivetrain on reflected inertia, making it difficult to compare motor/drive-train architectures for a given application.

To improve comparison across motors we normalize speed rate by the application-specific reflected inertia, expanding the speed rate into a relation we define as the *Reflected Speed Rate* (RSR):

$$RSR = \frac{K_m}{J_m N_{max}^2} \tag{20}$$

where, units are $[\frac{Nm}{\sqrt{W}\cdot Kg\cdot m^2}]$, $N_{max} = \frac{max(|\tau_l|)}{\tau_o}$ is the maximum gear reduction required to achieve the maximum target output torque τ_l, and τ_o is still motor stall torque.

D. Energetic Studies

The series spring in the SEA improves the power and energetic response of the motor [9], [35]. To understand how the series spring affects the actuator response, we took the nominal spring stiffness output from the optimization and compared it against a spring 50% stiffer and an effectively rigid spring with three orders of magnitude greater stiffness.

Sweeping across transmission ratio N, series spring stiffness K_s, parallel spring stiffness K_p, and parallel spring engagement point X_{p0} and evaluating motor voltage and current response we generated COT surface and contour maps for both knee and ankle target trajectories, similar to the method in [3]. The graphical mapping of parameters builds understanding of the relationships between actuator components. We utilized the RSR (20) to identify candidate motors for these studies, ultimately settling on the U10 Plus Kv100 from T-motor [36] for our analyses.

We built a powered ankle prosthesis, described in [24] as TF8, and tested it with a human subject to validate our simulation models. Human subject testing followed a protocol approved by an independent review board, the MIT Committee On Use of Human Experimental Subjects. A male, 75 kg, human subject was asked to walk on an instrumented treadmill at a set speed of 1.5 m/s wearing our TF8 ankle actuator. We measured joint angle, joint torque, motor voltage and motor current. We calculated the cumulative power consumption across a series of gait cycles to evaluate system energetics. A total of 28 gait strides were collected, their mean and standard deviation were then compared to our simulation data. The configuration tested included a 378 kN/m series spring, and no parallel spring.

III. Results

A. Series Stiffness

Series elasticity can improve power delivery at the output by storing and releasing energy in cyclical maneuvers. In Fig. 4 (a) we plot the motor torque/speed (top) and power (bottom) constraints. The solid red line is the physical limitation of the motor, below this line is technically achievable though not including thermal behavior considerations. The dotted lines of increasing density represent motor trajectories when three springs of increasing stiffness are each coupled in series with the actuator: $K_s = 271\frac{kNm}{m}, 344\frac{kNm}{m}$, and $271\frac{MNm}{m}$.

In Fig. 4(b) joint kinetics are shown in solid red, and again increasing stiffness series springs are represented as the increasing dot density plots. The right axis and red lines are the mechanical kinetics of the joint. The top figure showing travel the screw, followed below by the mechanical output

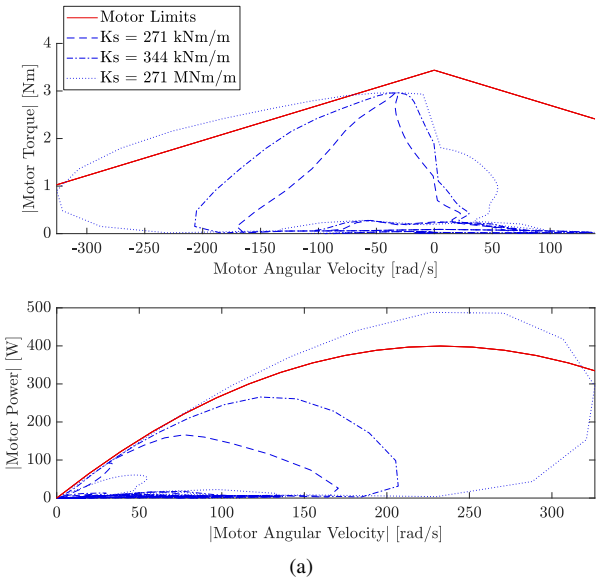

(a)

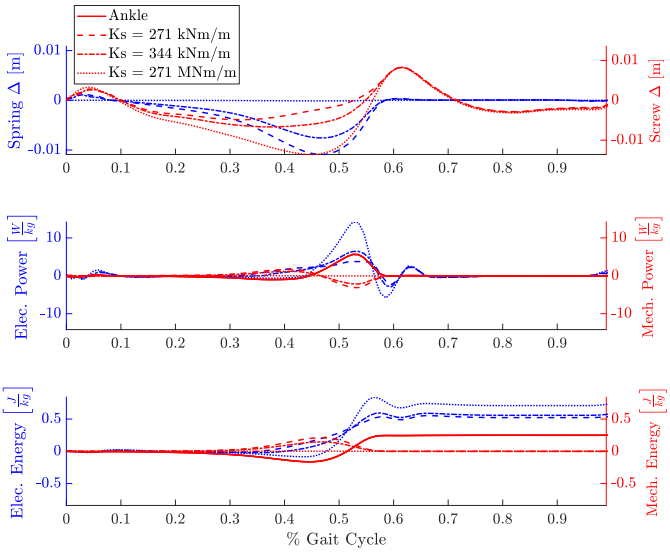

(b)

Fig. 4. Effects of series spring stiffness on motor performance and ankle gait energetics for 90kg user walking at 2.0 m/s. (a) The linearized model of motor capacity is shown against the performance of the actuator with varying series elasticity. Increasing stiffness begins to saturate motor capabilities. (b) Spring deflection affect on both electrical and mechanical energetics.

power of the joint, and the cumulative mechanical energy of the joint and series springs. The left blue axes and associated dotted lines are from top to bottom: the spring displacement of the actuator, electric power at the motor, and cumulative electric energy at the motor (including dissipative losses). Three nominal spring stiffnesses are shown, a light, heavy and effectively rigid structure. The optimal spring according to Fig. 4(a) reduces motor power and distance traveled requirements by 50% and overall energy consumption by about 30% compared to an actuator without series stiffness.

Preliminary data from level-ground walking experiments with the TF8 actuator show alignment with estimates. Fig. 5 is cumulative electric energy measured at the motor leads compared to simulated data for an equivalent mass subject. Simulated data expected 35 J per gait cycle, while measured mean data resulted in 28 J with a standard deviation of 4.9 J. We expect this variation between experiment and simulation is due to the difference in utilizing a finite-state machine controller, rather than true biological waveform. Additionally, this being preliminary data, we expect further tuning of the low-level control algorithms to improve torque tracking performance.

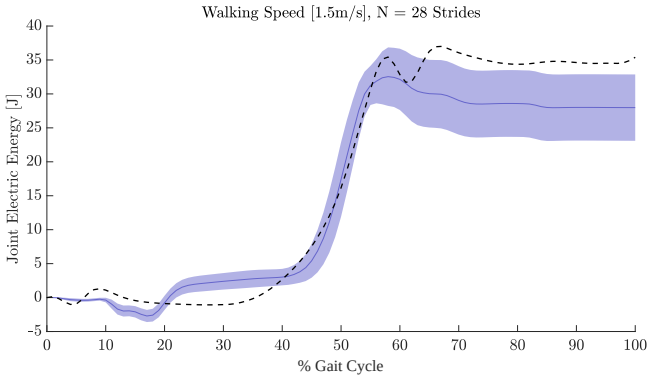

Fig. 5. Preliminary validation of the model with our ankle actuator described in [24] with a human test subject. User mass is 75 kg, walking 1.5 m/s, and K_s = 378 $\frac{kNm}{m}$. Solid line is mean, with purple shading showing one standard deviation from 28 strides. Estimated data is shown as dotted line.

B. Parallel Stiffness

Contour and surface maps of reduction ratio and series stiffness affects on system energetics for stair descent, level-ground and stair ascent of a biological ankle joint are shown in Figs. 6. Sub-figures (a-c) do not include a parallel spring, while (d-f) include a nominal parallel spring of $K-P = 3.59\frac{Nm}{rad \cdot kg}$. This parallel spring value came out of a parameter search and was found to be more energetically favorable than larger value from (18). The larger K_p values are found to be effective at level-ground walking, but counter-productive when the motor must overcome the force of the spring for changing stride lengths and terrains. The parallel spring does provide up to 8% improvement in energy expenditure. Optimal transmission ratio is about 60:1 but shifts towards higher ratios for stair ascent.

C. Knee

Level-ground walking of the knee joint in Fig. 7(a) shows a near zero electric energy cost and optimal reduction ratio of 35:1. One might expect greater energy regeneration in the knee with (b) showing negative mechanical energy at the joint being as much as -0.15 $\frac{J}{kg}$. The kinematically clamped analysis forces the knee to fully accelerate and decelerate itself, the

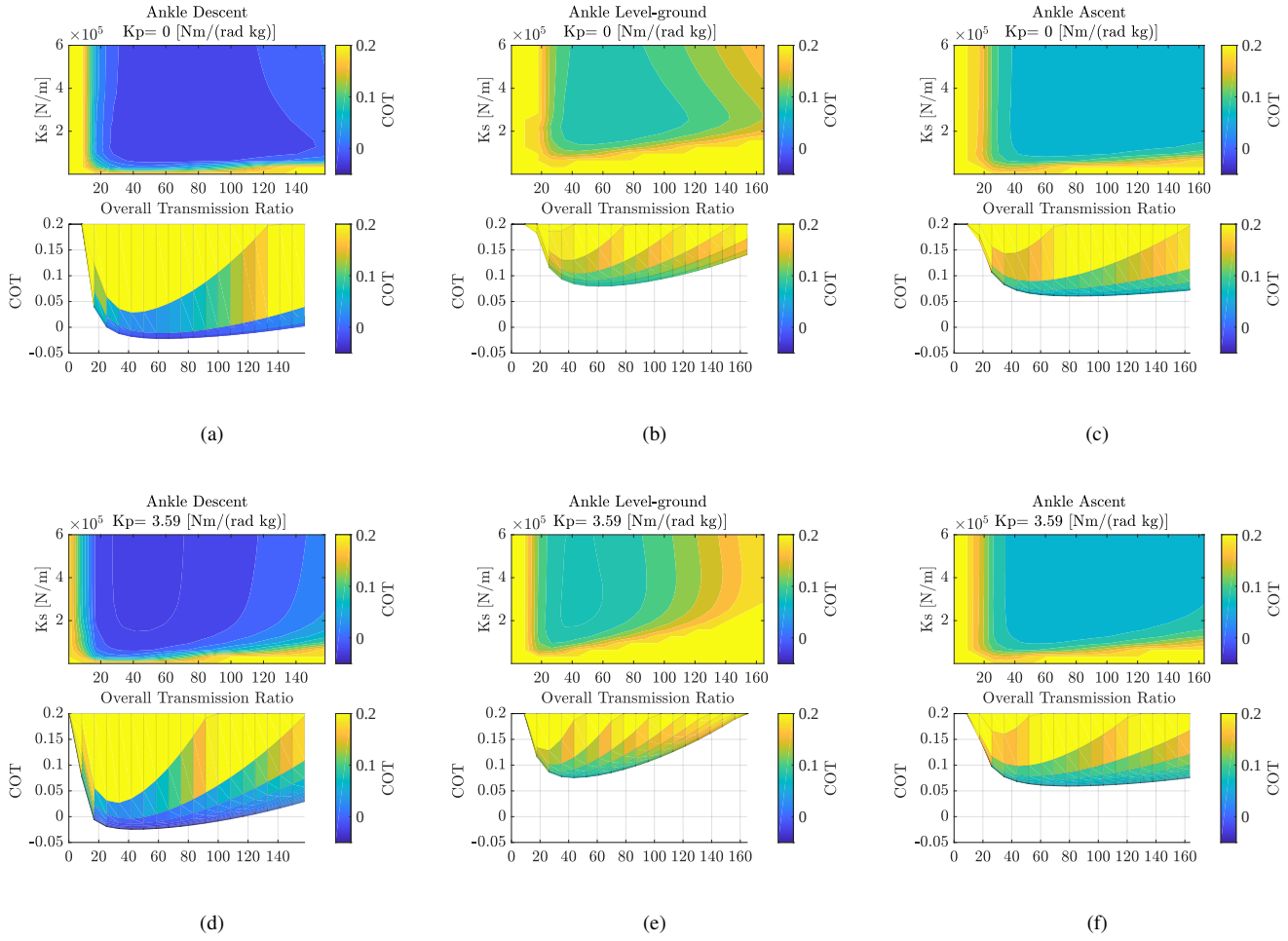

Fig. 6. Contour plots of the COT for one gait cycle are affected by series spring and parallel spring stiffness and overall transmission ratio. These analyses are based on the final choice of motor: TMotor U10 kV100 Plus. (a-c) show stair descent, level-ground walking, and stair ascent, respectively with no parallel spring. (d-f) show stair ascent, level-ground, and stair ascent, respectively with a parallel spring $K_p = 3.59 \frac{Nm}{rad \cdot kg}$, where we normalize by subject mass.

large spikes in the power curve in (b), however, in reality this motion is coupled with hip swing in addition to the knee.

D. Limited Range of Motion

The single largest improvement in actuator energy consumption is the case when dorsiflexion is restricted, as is the case with the BiOM. A 35% energy reduction is realizable when dorsiflexion is limited to 1° in energy configuration map Fig. 8.

IV. Discussion

The largest affects on system energetics are reducing range of motion, on-the-fly adjustment of reduction ratio for varied tasks and the inclusion of a moderately stiff parallel spring. Spring stiffness changes are also beneficial but are not as task dependent as we initially expected. Adjusting series spring stiffness between larger and smaller mass walking subjects can produce an improved energetic outcome, but across moderate changes in mass the energetic improvement is not substantial: e.g. a 90kg person walking on a spring specified for a 75kg user results in a 7 % increase in COT. Limiting range of motion has the single largest reduction in energy cost, but also affects the natural kinematics of a user. The trade-off in exchanging walking time for user feel is a consideration that should be considered based on desired user outcomes.

A varying reduction ratio could benefit task changes from level-ground walking to stair ascent. In level-ground walking an optimal reduction is about 60:1. In stair ascent the optimal reduction shifts to about 85:1 for the given motor. This shift is even more pronounced when a parallel spring is also included where the shift is from 45:1 to about 80:1 where there could be about 10% energy improvement between level walking and stair ascent. Screw driven actuators naturally vary their reduction ratio as the moment arm passes along the swept arc of the rotary output joint. Designs should be careful to recognize that decreasing screw ratios quickly ramp into steep energetic consequences. This should be considered in designs, or the linkage geometry itself should also be optimized according to gait trajectories.

The unidirectional parallel spring at the ankle can provide about 8% electric COT improvement across level-ground and

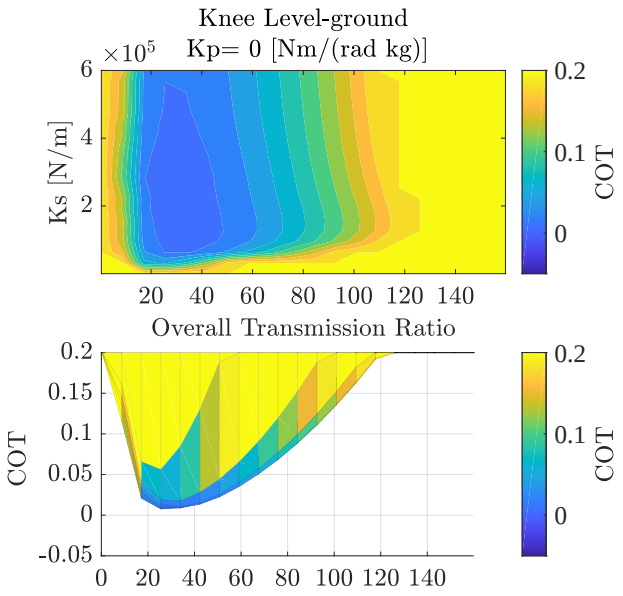

(a)

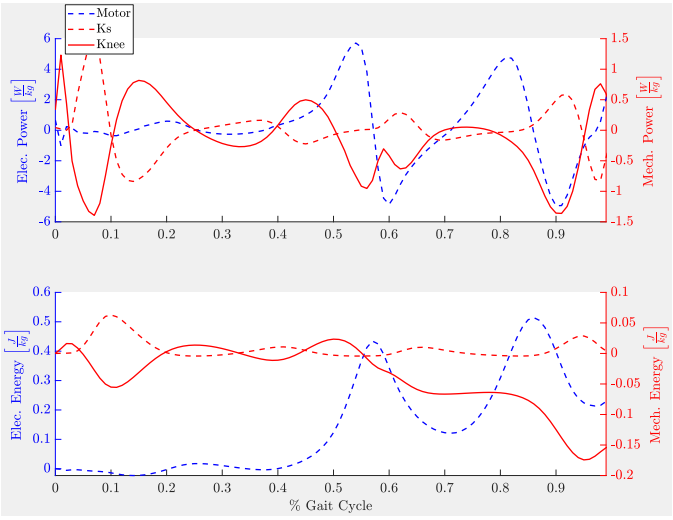

(b)

Fig. 7. (a) Energetic map for a knee actuator, and (b) the cumalative energy along a gait cycle for level-ground walking.

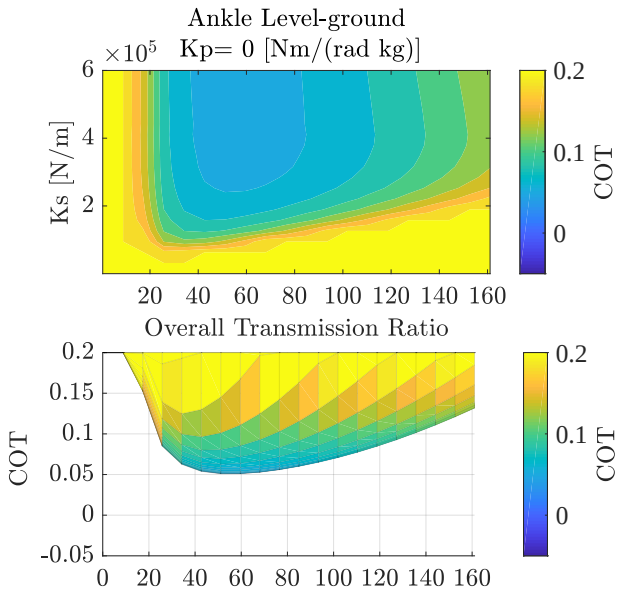

Fig. 8. When an actuator is limited to full plantarflexion but only one degree of dorsiflexion as is the BiOM, there is $\leq 30\%$ energy savings for level-ground walking compared to biological range of motion.

stair ambulation. Selection of the parallel spring stiffness is crucial. Too stiff of a spring is actually more energetically costly when the motor must overcome the parallel spring as in large range of motion maneuvers or slower walking speeds. Too soft of a spring does not cost energy, but also does not provide substantial energetic improvement considering the increased complexity and mass.

The knee does not benefit from a parallel spring. Fig. 7(b) helps show that the first order approximation of the knee is a damper: net energy is negative for each gait cycle. In mechatronics there is a chance this energy can be redistributed through the power bus, however, due to power transfer inefficiencies and the energy required to accelerate and decelerate the knee shank this behavior is not observed in this analysis. The series spring contributes to flattening of the motor energy for the first half of the gait cycle, but electric energy is consumed during the acceleration and deceleration of the knee in swing. The parallel spring contributes a load reduction during a negative energy portion of a gait cycle, quickly followed by a large positive energy gait phase, such as in the ankle. The knee, though, does not express this type of behavior during level-ground walking leaving the parallel spring a hindrance to motion. Potentially a clutched parallel spring could be utilized in stair ascent or descent, this could be evaluated in future analyses.

A set of maps that was not included in this paper are the infeasible operating zones for these energetic maps. Infeasibility is defined by the constraints defined in (15,16) and Fig. 4 and can be used to disallow configurations that can not be achieved. These results severely limit the operating regimes and clearly define operating specifications, but they limit clarity in visualizing the energetic maps, so they are left for the reader to apply their own design process.

V. Conclusions

These simulations help to understand the design space and to specify hardware configurations that can achieve specific task targets. The kinematic clamped analysis is a good starting point however we would recommend future design attempts to utilize a more sophisticated actuator model that includes controller effort. The process of disqualifying designs based on behavior that fails search constraints may be limiting when controller effort could allow generally better agreed behavior across the wider trajectory with torque, velocity or motor current and voltage saturation at only a few data points. Further, inclusion of a dynamic system model with

control effort could potentially give better understanding of final system response.

Realization of hardware can force variance from target component specifications. Limitations in commercially available components such as ideal gear ratios and springs can force a design away from strictly optimal configurations. In this analysis we provide a means to understand the design trade-offs in addition to a means to search for ideal components. Strict adherence to optimization results can leave one blind to feasible or infeasible design regimes. These two tools together, the energetic map and optimization procedures can provide insight into design trade-offs for future actuator architectures. Our own application of these methods are demonstrated in hardware in an accompanying paper [24].

ACKNOWLEDGMENT

The authors would also like to thank our funding sources for enabling this research, and our colleagues in the field contributing to the greater knowledge.

REFERENCES

[1] D. A. Winter, *The biomechanics and motor control of human gait.*, 1987.
[2] T. F. Novacheck, "Walking, Running, and Sprinting: a three-dimensional analysis of kinematics and kinetics." in *Instructional Course Lectures*, 1995, vol. 44, pp. 497–506.
[3] S. K. Au and H. M. Herr, "Powered Ankle-Foot Prosthesis," *IEEE Robotics & Automation Magazine*, no. September, pp. 52–59, 2008.
[4] H. M. Herr and A. M. Grabowski, "Bionic ankle–foot prosthesis normalizes walking gait for persons with leg amputation," *Proc. R. Soc. B*, vol. 279, no. 1728, pp. 457–464, feb 2012.
[5] R. E. Quesada, J. M. Caputo, and S. H. Collins, "Increasing ankle push-off work with a powered prosthesis does not necessarily reduce metabolic rate for transtibial amputees," *Journal of Biomechanics*, vol. 49, no. 14, pp. 3452–3459, 2016.
[6] R. Gailey, "Review of secondary physical conditions associated with lower-limb amputation and long-term prosthesis use," *The Journal of Rehabilitation Research and Development*, vol. 45, no. 1, pp. 15–30, 2008.
[7] Bionx, "The BiOM Advantage - BionX Medical Technologies," 2017.
[8] Össur, "Össur Dynamic Solutions Power Knee^{TM}," 2018.
[9] G. Pratt, M. M. Williamson, and Others, "Series elastic actuators," vol. 1. IEEE, 1995, pp. 399–406.
[10] S. K. Au, J. Weber, and H. Herr, "Biomechanical Design of a Powered Ankle-Foot Prosthesis," in *IEEE 10th International Conference on Rehabilitation Robotics*, 2007, pp. 298–303.
[11] P. Cherelle, V. Grosu, A. Matthys, B. Vanderborght, and D. Lefeber, "Design and validation of the ankle mimicking prosthetic (AMP-) Foot 2.0," *IEEE Transactions on Neural Systems and Rehabilitation Engineering*, vol. 22, no. 1, pp. 138–148, 2014.
[12] P. Cherelle, V. Grosu, M. Cestari, B. Vanderborght, and D. Lefeber, "The AMP-Foot 3, new generation propulsive prosthetic feet with explosive motion characteristics: Design and validation," *BioMedical Engineering Online*, vol. 15, no. 3, pp. 21–36, 2016.
[13] R. D. Bellman, M. A. Holgate, and T. G. Sugar, "SPARKy 3: Design of an active robotic ankle prosthesis with two actuated degrees of freedom using regenerative kinetics," *Proceedings of the 2nd Biennial IEEE/RAS-EMBS International Conference on Biomedical Robotics and Biomechatronics, BioRob 2008*, pp. 511–516, 2008.
[14] M. A. Holgate, J. K. Hitt, R. D. Bellman, T. G. Sugar, and K. W. Hollander, "The SPARKy (spring ankle with regenerative kinetics) project: Choosing a DC motor based actuation method," *Proceedings of the 2nd Biennial IEEE/RAS-EMBS International Conference on Biomedical Robotics and Biomechatronics, BioRob 2008*, pp. 163–168, 2008.
[15] M. Grimmer, M. Holgate, J. Ward, and A. Boehler, "Feasibility study of transtibial amputee walking using a powered prosthetic foot," in *International Conference on Rehabilitation Robotics (ICORR)*, 2017, pp. 1118–1123.
[16] R. M. Alexander, "Energy-saving mechanisms in walking and running." *The Journal of experimental biology*, vol. 160, pp. 55–69, 1991.
[17] D. Paluska and H. Herr, "The effect of series elasticity on actuator power and work output: Implications for robotic and prosthetic joint design," *Robotics and Autonomous Systems*, vol. 54, pp. 667–673, 2006.
[18] J. Zhu, H. She, and Q. Huang, "PANTOE II: Improved Version of a Powered Transtibial Prosthesis With Ankle and Toe Joints," in *Proceedings of the 2018 Design of Medical Devices Conference*. Minneapolis, MN, USA: ASME, 2018, pp. 1–3.
[19] H. M. Herr and A. M. Grabowski, "Bionic ankle-foot prosthesis normalizes walking gait for persons with leg amputation," *Proceedings of the Royal Society B: Biological Sciences*, vol. 279, no. 1728, pp. 457–464, 2012.
[20] E. S. Gardinier, B. M. Kelly, J. Wensman, and D. H. Gates, "A controlled clinical trial of a clinically-tuned powered ankle prosthesis in people with transtibial amputation," *Clinical Rehabilitation*, vol. 32, no. 3, pp. 319–329, 2018.
[21] J. R. Jeffers and A. M. Grabowski, "Individual Leg and Joint Work during Sloped Walking for People with a Transtibial Amputation Using Passive and Powered Prostheses," *Frontiers in Robotics and AI*, vol. 4, no. December, pp. 1–10, 2017.
[22] J. Schwartz, "A Brand-New Kick: The New BiOM Ankle Prosthetic by MIT's Hugh Herr," *Boston MAgazine*, nov 2013.
[23] A. D. Kuo, "A simple model of bipedal walking predicts the preferred speed-step length relationship." *Journal of biomechanical engineering*, vol. 123, no. 3, pp. 264–269, 2001.
[24] M. E. Carney and H. M. Herr, "Design of a Reaction Force Series Elastic Actuator for Powered Knee and Ankle Prostheses," 2019.
[25] T. Verstraten, J. Geeroms, G. Mathijssen, B. Convens, B. Vanderborght, and D. Lefeber, "Optimizing the power and energy consumption of powered prosthetic ankles with series and parallel elasticity," *Mechanism and Machine Theory*, vol. 116, pp. 419–432, 2017.
[26] S. Wang, C. Meijneke, and H. van der Kooij, "Modeling, design, and optimization of Mindwalker series elastic joint," jun 2013, pp. 1–8.
[27] E. J. Rouse, L. M. Mooney, and H. M. Herr, "Clutchable series-elastic actuator: Implications for prosthetic knee design," *The International Journal of Robotics Research*, vol. 33, no. 13, pp. 1–15, nov 2014.
[28] J. Markowitz, "A Data-Driven Neuromuscular Model of Walking and its Application to Prosthesis Control," Ph.D. dissertation, Massachusetts Institute of Technology, 2013.
[29] A. Protopapadaki, W. I. Drechsler, M. C. Cramp, F. J. Coutts, and O. M. Scott, "Hip, knee, ankle kinematics and kinetics during stair ascent and descent in healthy young individuals," *Clinical Biomechanics*, vol. 22, no. 2, pp. 203–210, 2007.
[30] E. J. Rouse, L. M. Mooney, E. C. Martinez-Villalpando, and H. M. Herr, "A Clutchable Series-Elastic Actuator: Design of a Robotic Knee Prosthesis for Minimum Energy Consumption," in *Proceedings of the IEEE International Conference on Rehabilitation Robotics*, 2013.
[31] V. L. Orekhov, C. S. Knabe, M. A. Hopkins, and D. W. Hong, "An unlumped model for linear series elastic actuators with ball screw drives." IEEE, 2015, pp. 2224–2230.
[32] C. E. Clauser, J. T. McConville, and J. W. Young, "Weight, Volume, and Center of Mass of Segments of the Human Body," *National Technical Information Service*, pp. 1–112, 1969.
[33] T. Verstraten, R. Furnémont, G. Mathijssen, B. Vanderborght, and D. Lefeber, "Energy Consumption of Geared DC Motors in Dynamic Applications : Comparing Modeling Approaches," vol. 1, no. 1, pp. 524–530, 2016.
[34] J. W. Sensinger, "Selecting motors for robots using biomimetic trajectories: optimum benchmarks, windings, and other considerations," *Proceedings - IEEE International Conference on Robotics and Automation*, pp. 4175–4181, 2010.
[35] D. Paluska and H. Herr, "Series elasticity and actuator power output," *Proceedings - IEEE International Conference on Robotics and Automation*, vol. 2006, no. May, pp. 1830–1833, 2006.
[36] T-Motor, "T-Motor," 2017.